Cellular Terrestrial Broadcast—Physical Layer Evolution From 3GPP Release 9 to Release 16

Ayan Sengupta, Alberto Rico Alvarino, Amer Catovic, and Lorenzo Casaccia

***Abstract*—We present the latest developments in the physical layer evolution for the transmission of Multimedia Broadcast Multicast Service (MBMS) over fifth generation (5G) cellular networks. We first provide an overview of how the MBMS physical layer has evolved during the initial releases of the Third Generation Partnership Project (3GPP) specifications and provide motivations and insights for key developments that have helped mature MBMS into a competitive broadcasting solution. We provide an overview of dedicated MBMS carriers for Multimedia Broadcast multicast service Single Frequency Network (MBSFN) transmission as well as Orthogonal Frequency Division Multiplexing (OFDM) numerologies with longer cyclic prefixes to support MBSFN transmission over large geographical areas with large distances between cooperating cell sites. Next, we describe the most recent enhancements to the MBMS physical layer, addressing advanced use cases in the recently completed release of the 3GPP specifications (Release 16). First, we describe the physical layer design for enabling MBSFN-based MBMS services for rooftop receivers with inter-site distances between cooperating cell sites as large as 125 km. In this realm, we demonstrate the need for an OFDM numerology with a 300-microsecond cyclic prefix to communicate effectively over channels with very large delay spreads. Next, we explain how support for high mobility up to 250 kmph was added to the standards by using an OFDM numerology that gracefully trades off inter-symbol interference due to large delay spreads and inter-carrier interference due to large doppler spreads to achieve better performance than existing numerologies at high speeds. Finally, we describe the enhancements that were made to the Cell Acquisition Subframe (CAS)—specifically, the introduction of larger aggregation levels for the Physical Downlink Control Channel (PDCCH) and the support of Physical Broadcast Channel (PBCH) repetitions—that significantly increase the coverage for the control and system information associated with MBMS that are carried by these subframes.**

***Index Terms*—MBMS, eMBMS, FeMBMS, MBSFN, physical layer, 3GPP, 5G, broadcast, multicast, LTE.**

I. Introduction

FOURTH generation Long-Term Evolution (4G-LTE) and fifth generation (5G) cellular networks have, over the years, expanded in scope to support several new verticals besides mobile broadband. Some examples of this expansion can be witnessed in the realm of massive machine-type communications (mMTC), ultra-reliable low-latency communications (UR-LLC), connected automobiles (Cellular vehicle-to-everything or C-V2X), industrial Internet-of-Things (IIoT) and many others. This is made possible by leveraging the flexible Orthogonal Frequency Division Multiplexing (OFDM)-based physical layer architecture of cellular networks, that can be adapted to different use cases and requirements.

One such area in which cellular networks have evolved from the 4G-LTE days is in the realm of cellular broadcast—referred to in the Third Generation Partnership Project (3GPP) specifications for cellular communication [4], [5] as Multimedia Broadcast Multicast Service (MBMS). MBMS provides an attractive solution to the broadcasting industry, since it enables broadcasters to reach the billions of cellular devices (User Equipments or UEs) that exist and operate on the 3GPP standards for cellular communication. In this paper, we describe the key elements in the evolution of the physical layer for MBMS—from the early releases of the 3GPP specifications to present-day specifications that are designed to meet the requirements for broadcasting in 5G, as laid out in [1].

The physical layer specifications for MBMS are primarily based on a transmission technique termed Multimedia Broadcast multicast service Single Frequency Network (MBSFN) transmission. With MBSFN, several cells across a (potentially large) geographical area synchronously cooperate to deliver MBMS service to the UEs. This form of cooperative transmission allows for extremely large coverage areas—for example, nationwide coverage—which is an attractive attribute from a broadcasting point-of-view. In addition to MBSFN-based MBMS transmission, 3GPP specifications also provide support for a single cell-based broadcasting solution (Single Cell Point to Multipoint or SC-PTM) that is useful for broadcasting or multicasting to a set of UEs that are localized in a small geographical area. In this paper, we will be dealing primarily with MBSFN-based MBMS evolution, that is designed to meet the needs of broadcasters to transmit content across large geographical areas.

The first set of specifications for the MBMS physical layer (in 3GPP Release 9), also referred to as evolved MBMS (eMBMS), were based on *time-sharing* the available operator-controlled resources between unicast and multicast/broadcast traffic, thereby limiting the throughput that can be achieved for MBSFN transmission. Moreover, the OFDM *numerologies* (including the duration of the

Manuscript received December 16, 2019; revised March 23, 2020; accepted March 27, 2020. Date of publication May 6, 2020; date of current version June 5, 2020. *(Corresponding author: Ayan Sengupta.)*

Ayan Sengupta, Alberto Rico Alvarino, and Amer Catovic are with the Qualcomm Standards and Industry Organization, Qualcomm Technologies Inc., San Diego, CA 92121 USA (e-mail: asengupt@qti.qualcomm.com; albertor@qti.qualcomm.com; amerc@qti.qualcomm.com).

Lorenzo Casaccia is with the Qualcomm Standards and Industry Organization Spain, Qualcomm Europe, Inc., Spain Branch Office, 28108 Alcobendas, Spain (e-mail: lorenzoc@qti.qualcomm.com).

Color versions of one or more of the figures in this article are available online at http://ieeexplore.ieee.org.

Digital Object Identifier 10.1109/TBC.2020.2986922

cyclic-prefix and subcarrier-spacing) were like that of legacy LTE and were not designed to handle channels with large delay spreads that arise when cooperating MBSFN transmitters are separated by large geographical distances. As a first step towards addressing these needs, 3GPP Release 14 introduced support for a dedicated MBMS carrier for MBSFN transmission that could be deployed in spectrum owned and controlled by the broadcasters. This was also accompanied by simplification and streamlining of the control and system-information acquisition, thereby freeing up most of the available resources for MBSFN transmission. Another major step towards evolving MBMS for large-area terrestrial broadcast scenarios in Release 14 was the introduction of an OFDM numerology with a long cyclic prefix duration of 200 microseconds. This was a key enabler for the usage of MBSFN transmission in broadcaster-deployed networks with inter-site distances of in excess of ten kilometers between cooperating transmitters—both for fixed rooftop receivers as well as car-mounted receivers with some degree of mobility. Collectively, the Release 14 MBMS enhancements are referred to as Further evolved MBMS (FeMBMS).

While the Release 14 physical layer specifications for MBSFN-based MBMS paved the way for evolving MBMS into the 5th generation of cellular networks, there were still use cases that needed to be addressed and requirements that needed to be met to satisfy all the requirements of 5G cellular broadcast as laid out in [1]. The evolution that took place to address these requirements are based on the LTE air interface—hence, this evolution is referred to under the moniker of *LTE-based 5G Terrestrial Broadcast* in 3GPP Release 16.

The first among these Release 16 enhancements was the support of MBSFN transmission with rooftop receivers in High Power High Tower (HPHT) and Medium Power Medium Tower (MPMT) settings [1], [2], where the distances between cooperating cell sites may be as large as 125 kilometers. As we will demonstrate in Section IV of this paper, this requires the introduction of an OFDM numerology with an even larger cyclic prefix (which provides a system-level SNR gain of up to 7.3 dB over the previously specified numerologies) and a sparser arrangement of reference signals (pilots) in the time-frequency grid to achieve spectral efficiencies in the range of 2 bits/sec/Hz with 95-99% UE coverage at a physical layer block error rate (BLER) of 1%.

The second requirement that needed to be addressed was the support of MBMS reception with car-mounted antennas in high mobility scenarios of up to 250 kmph. While Release 14 addressed some aspects related to supporting mobility, tackling the extreme doppler spreads that result from such high speeds, together with the large channel delay spreads from moderately large inter-site distances between 10 and 50 kilometers, requires support for a new OFDM numerology that achieves a good tradeoff in handling inter-symbol interference (ISI) and inter-carrier interference (ICI) to provide improved spectral efficiencies for MBMS reception that were previously not achievable. We describe the physical layer evolution in the regard in Section V of this paper.

Third, there was a need to improve the coverage of the control and system-information channels for MBMS services, that are carried by *Cell Acquisition Subframes* (CASs). It is critical for a UE interested in receiving MBSFN-based MBMS services to reliably receive the CAS under a variety of scenarios. In Section VI of this paper, we present the various enhancements that were made to the Physical Downlink Control Channel (PDCCH), Physical Broadcast Channel (PBCH) and the Physical Control Format Indicator Channel (PCFICH) within the CAS, that enables UEs in previously coverage-limited scenarios to reliably received the CAS 99% of the time with a physical layer BLER of 1%.

A. Related Literature

In addition to the 3GPP Technical Reports (TRs) and technical contributions [1]–[5], [8]–[9], [12]–[14], several articles cover various aspects related to the evolution, ongoing development and potential future enhancements to 3GPP-based cellular broadcasting systems. Among them, [15], [16] provide detailed overviews and evaluations on eMBMS. Reference [17] studies the impact of long cyclic prefixes in eMBMS networks, while [18] evaluates the performance of several potential physical layer enhancements to eMBMS, including layered division multiplexing. References [19], [20] presents an overview of Release 14 FeMBMS and provides performance evaluations under different settings. References [21], [22] present contemporary work on Release 16 enhancements to 3GPP-based cellular broadcast. References [23]–[25] examine various aspects related to future 5G New Radio (NR)-based deployment and operation of cellular broadcast networks. In the realm of competing broadcast-centric standards, [26] provides an overview of the Digital Video Broadcasting—Second Generation Terrestrial (DVB-T2) standard while [27] describes the physical layer of the Advanced Television Systems Committee (ATSC) 3.0 standard.

B. Organization of the Paper

The rest of this paper is organized as follows: In Section II, we provide an overview of how the physical layer for MBMS has evolved from the early releases of 3GPP specifications, up to Release 14. In Section III we describe, at a high level, the most recent enhancements that were made to MBSFN-based MBMS transmission in 3GPP Release 16; in the following sections, we describe each of these enhancements in detail. Section IV presents the physical layer design for enabling rooftop MBMS reception with very large (up to 125 km) inter-site distances between cooperating transmitters. Section V describes how support for high mobility up to 250 kmph was added. Section VI describes the various enhancements that were made to the channels in the CAS.

II. MBMS Physical Layer Evolution up to 3GPP Release 14

The Radio Access Network, comprising transmitters, receivers and the protocols for their communication, for supporting MBMS services in LTE dates to LTE Release 9. Initially MBMS transmission was time-multiplexed with unicast transmission across the available resources in a given

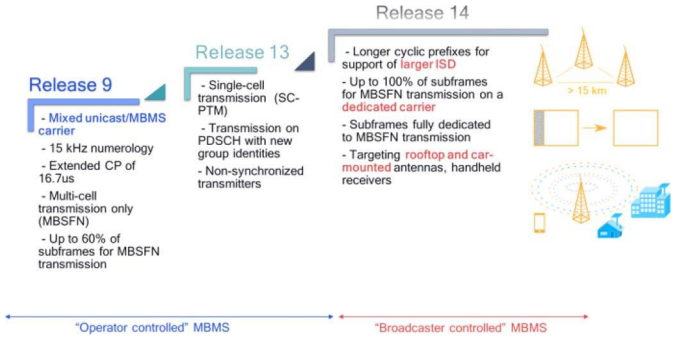

Fig. 1. Evolution of the MBMS Radio Access Network in 3GPP specifications up to Release 14. Common industry nomenclature for the evolutions of MBMS are evolved MBMS (eMBMS) in Release 9 and Further evolved MBMS (FeMBMS) in Release 14.

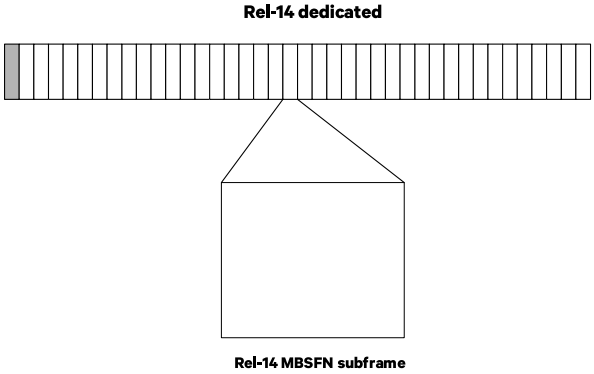

Fig. 2. 39 consecutive MPSFN subframes (in white) after a Cell Acquisition Subframe (in grey) in a dedicated MBMS carrier without control region(s) in the MBSFN subframes. In the illustration, one (MBSFN) subframe represents a time unit of 1 millisecond.

frequency carrier. In this setting, the cellular operator controlled the spectrum and traffic delivery.

In the initial LTE specifications, MBMS transmission was supported in an MBSFN framework—i.e., one where multiple synchronized base-stations cooperatively transmit over the same time-frequency resources, by forming a Single Frequency Network (SFN). The cooperating base stations that contribute to a given MBSFN transmission are said to form an MBSFN Area. Using this MBSFN approach for MBMS allows for transmission of MBMS services over very large geographical areas—an important use case for broadcast content delivery.

Subsequently, in Release 13, LTE specifications also added support for a single-cell based broadcast/multicast solution, referred to as Single Cell Point to Multipoint (SC-PTM) transmission. In this mode of transmission, data is multicast to groups of UEs using group-common identifiers, on the physical downlink shared channel (PDSCH). SC-PTM is most suited to scenarios where broadcast/multicast content only needs to be delivered to one or at most a few cells in a small geographical area. In this realm, SC-PTM proves to be quite flexible in dynamically adapting to the traffic needs in a cell. However, for terrestrial broadcast scenarios where (for example) TV services need to be provided to a large geographical area, cooperative transmission with MBSFN is potentially a more efficient option.

While the initial releases of LTE paved the way for broadcast/multicast transmission over cellular networks, some key ingredients were still required to meet the requirements of the broadcasters and support similar use cases as the competing broadcasting standards such as DVB-T2 [10], [26] and ATSC 3.0 [11], [27]. Chief among these were the idea of a broadcaster controlled dedicated MBMS carrier and numerologies to support larger (than typical cellular deployments) distances between cooperating MBSFN cells. Next, we provide an overview of these enhancements to MBMS that were made in Release 14. A depiction of the MBMS physical layer evolution up to Release 14 is shown in Fig. 1.

A. Dedicated MBMS Carrier

Support for a dedicated MBMS carrier was a key enabler of broadcaster controlled MBMS setups, wherein the spectrum for deploying the MBMS services is owned and controlled by the broadcasters, as opposed to shared MBMS and unicast services over spectrum that is owned and controlled by incumbent cellular operators. With support for a dedicated MBMS carrier, the throughput for MBMS services could be improved significantly, since now almost 100 percent (except the cell acquisition subframes, which are sparse in time) of the resources in the dedicated MBMS carrier are allotted for MBMS services. Also, as shown in Fig. 2, in a dedicated MBMS carrier setup, there are no control symbols in the form of a Physical Downlink Control Channel (PDCCH) outside the cell acquisition subframes—the entire MBSFN subframe is used for broadcast transmission. Before Release 14, in a mixed unicast/broadcast setup (simply referred to as a mixed carrier setup), a maximum of 60 percent of the subframes could be allocated for MBSFN transmission, and each subframe could potentially have associated control signaling.

To facilitate maximum throughput for MBSFN transmission in a dedicated MBMS carrier, the initial cell acquisition and control signaling were also streamlined to free up more resources to transmit broadcast data. In Fig. 3, we depict the synchronization and control signal structures for MBMS in both mixed carrier as well as dedicated MBMS carrier setups. As shown in Fig. 3, in a dedicated MBMS carrier, the synchronization signals (primary synchronization signal (PSS) and secondary synchronization signal (SSS)), as well as the Master Information Block (MIB) and System Information Blocks (SIBs) are transmitted together in a Cell Acquisition Subframe (CAS), which has a periodicity of 40 milliseconds. This leads to an effective fraction 39/40 = 0.975 of subframes that are dedicated to MBSFN transmission. To improve coverage of the channels in the CAS, signal combining across transmission time intervals (TTIs) are supported. The contents of the MIB and SIB are kept unchanged for 160 milliseconds, allowing for 4-TTI combining for MIB (carried in the physical layer by the Physical Broadcast Channel (PBCH)) and 2-TTI combining for SIB (carried in the physical layer by the Physical Downlink Shared Channel (PDSCH)).

B. Support of Larger ISDs—Numerology With 200 Microseconds Cyclic Prefix

Together with support for a dedicated MBMS carrier, support was introduced for an MBSFN numerology with a

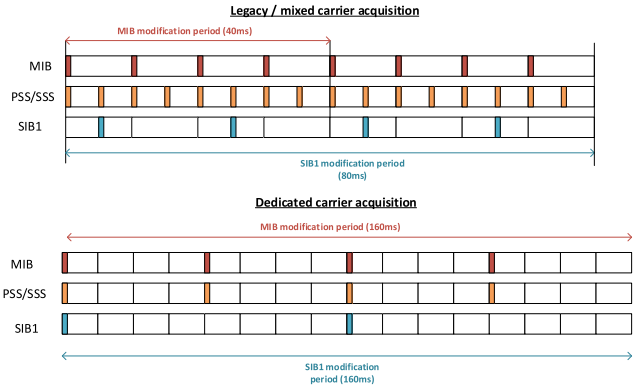

Fig. 3. Synchronization signal and system information structure in mixed versus dedicated MBMS carriers.

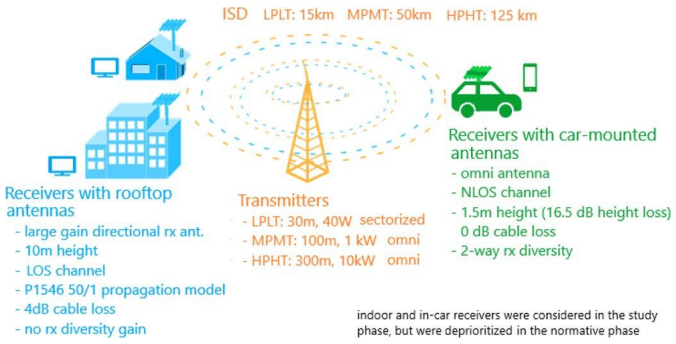

Fig. 4. Overview of MBMS enhancement use cases in 3GPP Release 16.

significantly longer (compared to what was specified before) cyclic prefix duration of 200 microseconds.

Unlike legacy cellular base-station deployments which are often dense, broadcaster-controlled networks typically have a sparser deployment of dedicated MBSFN base-stations spread out over a large geographical area over which MBMS services need to be provided. The distance between these MBSFN base-stations (referred to as the inter-site distance, or ISD) is typically in the range between 10 km and 150 km, sometimes even more. When these MBSFN base-stations cooperate to form an MBSFN Area, the resulting delay-spread of the channel that a receiver (user equipment, or UE) observes is rather large. To combat this large delay spread, the cyclic prefix duration of the OFDM symbols needs to be large enough, to minimize inter-symbol interference. This was the motivation in moving to a numerology with a 200-microsecond cyclic prefix, to at least provide enhanced support towards meeting some of these deployment challenges.

It is worthwhile to note, however, that the above numerology in Release 14 was primarily designed and best suited to provide support for ISDs of around 15 km. As we will show in the following sections, this numerology cannot adequately handle much larger ISDs up to 125 km in high-power high-tower scenarios. For these settings, a numerology with even longer cyclic prefix was necessitated in Release 16, that specifically caters to rooftop reception with ISDs up to 125 km.

III. Release 16 Enhancements—Overview

To evolve MBMS to address further new use cases in Release 16, there were three key areas identified, which we describe in this section. Some of these are depicted pictorially in Fig 4.

First was the support for large ISDs up to 125 km. This represents a significant leap in requirements from Release 14 and is tailored to provide rooftop reception in Medium Power Medium Tower (MPMT) as well as High Power High Tower (HPHT) settings (see Fig. 4). This would require designing an MBMS numerology that is capable of handling channels with much larger delay spreads than Release 14, owing to the larger ISDs supported.

Second was the support of high mobility—up to 250 kmph for mobile and portable UEs. While the Release 14 dedicated MBMS numerology provides good performance at low to moderate mobility, the 1.25 KHz subcarrier spacing is not capable of handling the large doppler spreads that result from high mobility. This would require a numerology that has a larger subcarrier spacing than the Release 14 numerology, thereby making it more resilient to doppler at high speeds.

Third, it was identified that under certain deployments and use cases (most notably, for car-mounted receivers in LPLT scenarios) that decoding the control channels (PDCCH and PBCH) in the Cell Acquisition Subframe (CAS) could become a bottleneck. To solve this problem, enhancements to the PDCCH and PBCH in the CAS are proposed in Release 16.

In the following sections, we provide more detail into each one of these three directions.

IV. Rooftop Reception With ISDs up to 125 km

A. Numerology With 300 Microseconds Cyclic Prefix

As described in Section III, the identified use cases for rooftop receivers have large inter-site distances between cooperating transmitters—up to 50 km for MPMT settings, and up to 125 km for HPHT settings. Owing to such large inter-site distances, the delay spread of the resulting channel at the receivers tend to be much higher than those that can be effectively contained within the 200-microsecond cyclic prefix of the Release 14 MBMS numerology. As a result, during the study item phase in Release 16, two numerologies with larger cyclic prefixes were identified as potential candidates for broadcasting to rooftop receivers, among which, a numerology with 300-microseconds cyclic prefix was adopted in the standards.

This adopted numerology (with 300-microseconds cyclic prefix and 2700-microseconds useful symbol duration, depicted in Fig. 5) has several favorable attributes. First, with a scheduling unit of one Physical Multicast Channel (PMCH) symbol, the scheduling boundaries align with the legacy LTE scheduling unit of 1 millisecond, which is attractive for mixed-carrier deployments with other technologies. Second, there are exactly 13 PMCH symbols between two consecutive CASs that are present every 40 milliseconds apart. Third, the Fast Fourier Transform (FFT) size required to implement this

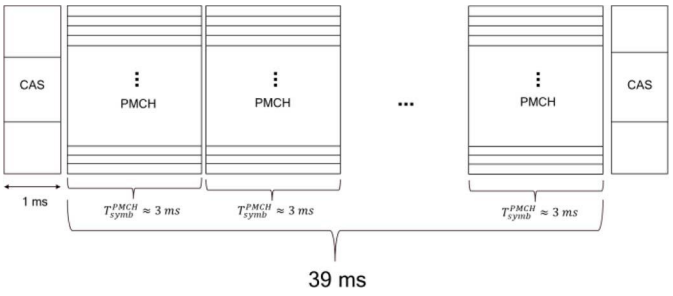

Fig. 5. MBSFN transmission with Physical Multicast Channel (PMCH) symbols of 3ms duration for rooftop MPMT and HPHT reception with up to 125 km ISD.

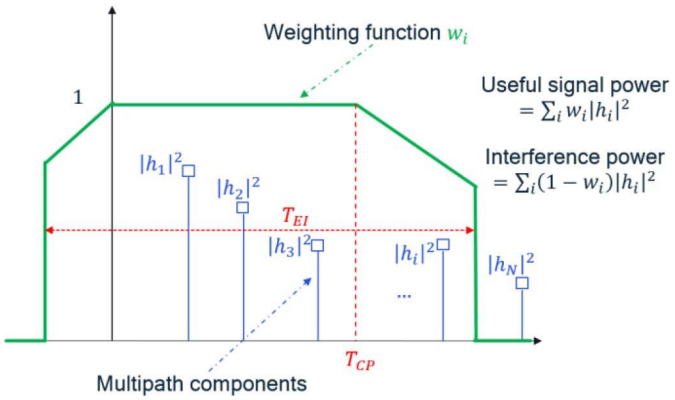

Fig. 6. Calculation of SNR from a multipath channel instance. The multipath components within the equalization window contribute to the received signal, while those outside it are treated as interference.

numerology can be represented as a product of powers of 2 and 3, which is attractive from an implementation standpoint.

B. System Level Evaluations

1) Channel Model: To perform system-level evaluations for the use cases of interest, we use the ITU-R P.1546-5 [6] channel model for path loss, as agreed in the simulation assumptions in [2]. In the modeling, the path loss of the serving cell is determined from the 50% time-variability curves in [6] for the corresponding carrier frequency, i.e., the field strength values that are exceeded 50% of the time are used. For the interfering cells, however, the 1% time-variability curves are used, i.e., the field strength values that are exceeded only 1% of the time. This is a conservative system modeling approach, which may result in situations where the signal from the serving transmitter is weaker than the interfering transmitter—a situation that a cellular receiver would try to avoid by reselecting to a stronger transmitter—but one that is generally preferred by the broadcasters. Shadowing and small-scale fading are also incorporated into the channel model, with parameters determined by the scenario (e.g., MPMT vs HPHT vs LPLT transmitters, rooftop vs car-mounted antennas). The detailed channel models for each scenario can be found in [2, Tab. 2].

2) SNR Calculation: The calculation of SNR from the realization of the channel is obtained likein [7, Sec. 3.5]. The signal energy within the *equalization window* is shaped by the weights w_i. while the energy outside the equalization window is treated as interference (i.e., $w_i = 0$). This is depicted pictorially with an example in Fig. 6. The *equalization window* is essentially equal to the length (in terms of delays) of the channel that can be measured by a certain pilot pattern in frequency. From the sampling theorem, an effective pilot (reference signal, or RS) spacing of 1 in every N subcarriers, results in an equalization window of $T_{EI} = \frac{1}{N \times SCS}$ where SCS denotes the subcarrier spacing of the numerology used for MBMS transmission.

3) Performance Evaluation: In Fig. 7 and 8, we show the system-level SNRs that we obtain for the MPMT and HPHT rooftop scenarios respectively with different numerologies. In each figure, we group the 95th percentile SNRs (i.e., the SNR level that at least 95 percent of the UEs experience) to the left, and the 99th percentile SNRs to the right. In the legends of Figs. 7 and 8, "Tcp/Tu/EI" refers to a configuration where the

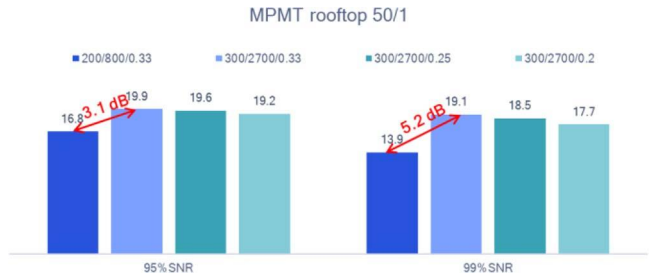

Fig. 7. System-level SNRs for the rooftop MPMT scenario with the 50/1 ITU-R P.1546-5 channel model with small-scale fading.

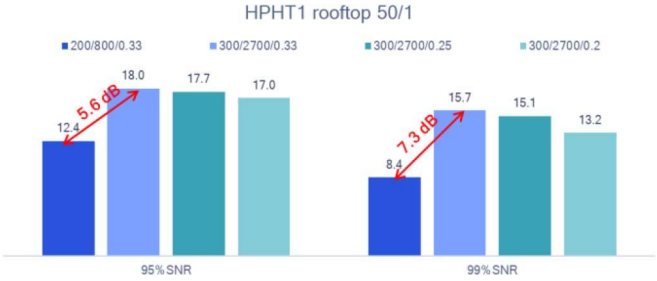

Fig. 8. System-level SNRs for the rooftop HPHT scenario with the 50/1 ITU-R P.1546-5 channel model with small scale fading.

cyclic prefix duration is Tcp microsecond, the useful symbol duration is Tu microseconds and the RS density in frequency (expressed as a fraction) is EI.

From Figs. 7 and 8, we see the clear benefits of the 300-microsecond CP numerology (over the Release 14 numerology with 200-microseconds CP) under both the rooftop scenarios under consideration. While the gains for the MPMT scenario range between 3.1 to 5.2 dB, those for the (larger ISD) HPHT scenario range from 5.6 dB to 7.3 dB. These gains are explained by the fact that a 200-microsecond CP is insufficient to provide adequate protection from inter-symbol interference when the channel delay spreads are very large. Moreover, as we will see later, the system-level SNRs achieved with the 300-microsecond numerology facilitate spectral efficiencies upwards of 1.5 bits/sec/Hz.

It is also worth noting that in the system-level results, an RS-density of 1/3 in the frequency domain provides the best

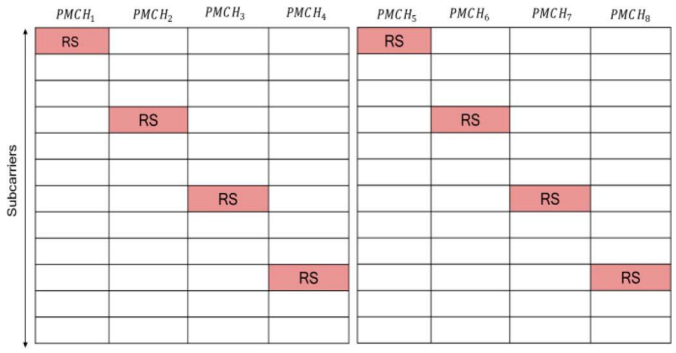

Fig. 9. Time-frequency staggering of Reference Signals (RSs) for Physical Multicast Channel (PMCH) transmission. Depicted RS pattern has a frequency spacing (F_d) of 3 subcarriers staggered across $T_d = 4$ symbols.

performance. However, as we will see in the link-level evaluations in the following sections, the system-level results do not provide insight into the "time-stagger" of these reference signals—i.e., whether it is better to put 1 RS out of every 3 subcarriers in every symbol, or to stagger is across say T_d symbols, where each symbol has an RS once in every $3 \times T_d$ subcarriers.

C. Reference Signal Pattern

While the system-level evaluations in the preceding section provide some insight on the equalization interval, here we perform link-level evaluations to determine the best RS patterns for the 300-microsecond numerology designed for rooftop reception.

An RS pattern with "Frequency Spacing" of F_d subcarriers and "Time Stagger" of T_d symbols implies that when the RSs from T_d consecutive symbols are coalesced together, there is an RS in one out of every F_d subcarriers throughout the entire system bandwidth. In other words, instead of putting an RS every F_d subcarriers in one (or each) symbol, we "stagger" these RSs across T_d symbols, to reduce overhead.

The optimal staggering parameter T_d depends on the Coherence Time of the channel—for channels that change quickly, we need smaller T_d values to effectively keep track of the channel. The design tradeoff is in balancing overhead reduction with channel estimation accuracy (due to Doppler). Additionally, a very large value of T_d may result in reduced performance in the presence of residual frequency error.

An RS pattern of $F_d = f, T_d = t$, has a base unit of $f \times t$ subcarriers and t symbols in the time-frequency plane, which then repeats as a block in time and frequency. Fig. 9 depicts a base unit of an RS pattern with $F_d = 3, T_d = 4$.

1) Reference Signal Staggering in Time: To evaluate the impact of different time-stagger parameters T_d on link-level performance, we ensure that for every time-stagger pattern evaluated, we perform cross-subframe channel estimation across the same number of PMCH symbols. In the simulation results we present here, for all values $T_d = 1, 2, 3, 4$ we perform cross-subframe channel estimation across 4 consecutive PMCH symbols. The channels model is TDL-E [3] (as per the simulation assumptions in [2]) with delay spreads of $45\mu s$ for HPHT and $35\mu s$ for MPMT scenarios.

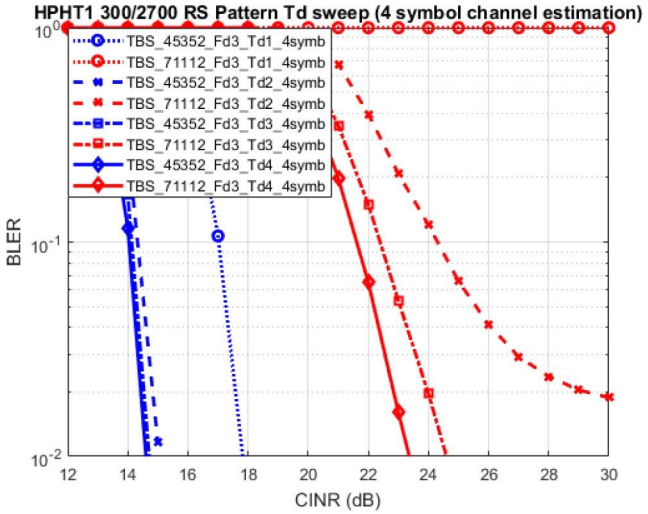

Fig. 10. Link-level performance with different time-stagger patterns for reference signals with the 300-microsecond CP numerology in the rooftop HPHT scenario. The channel estimation is performed using a sliding window-based 2D MMSE algorithm across 4 OFDM symbols and 4 resource blocks.

From Fig. 10, we observe that for the HPHT1 scenario with an RS density of $\frac{1}{3}$, a time stagger of 4 symbols provides the best performance. This can be explained by the fact that the Doppler Spread for the rooftop reception settings is very small, which results in an extremely slowly varying channel—as a result, the reference signals can be "spread out" across time, and still be combined together from all the symbols in the stagger pattern without noticeable channel estimation penalties, while, at the same time, reducing the net RS overhead considerably. As in evidenced from Fig. 10, the RS overhead savings with $T_d = 4$ translates to a greater than 4 *dB* improvement (at BLER $= 10^{-2}$) over $T_d = 2$ for larger TBSs, where for $T_d = 2$, error floors are observed that limit BLER performance.

2) Reference Signal Density in Frequency: While the system level simulations already pointed to a gain for the setting with an RS density of $\frac{1}{3}$ in frequency, we further obtain additional confirmation from our link-level simulations (shown in Fig. 11) that an (effective, combined across an entire "time stagger", as defined in the previously) RS density of $\frac{1}{3}$ provides the best link-level performance. Sparser RS densities in frequency ($F_d = 4, 5$) fail to estimate the (large delay-spread) channels in this setting.

3) Dual Support of $\mathbf{T_d = 4}$ *and* $\mathbf{T_d = 2}$ *for the RS Pattern:* While the benefits of a time-stagger parameter of $T_d = 4$ have been explained in this section, it is worthwhile to note that this performance requires the de-staggering of RSs from 4 consecutive PMCH symbols. There may be instances (for example, in mixed carrier settings, as described in [8]) where the availability of 4 consecutive PMCH symbols from the same MBSFN area may not be guaranteed. To cover for such cases, it was decided to support both $T_d = 4$ and $T_d = 2$ for the RS pattern staggering for the 300-microsecond CP numerology; the network has the option of configuring from among the two patterns.

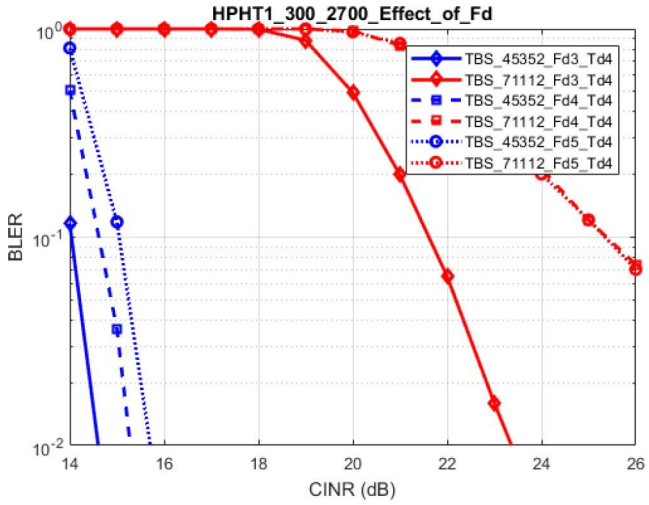

Fig. 11. Link-level performance with different frequency-spacings for reference signals with the 300-microsecond CP numerology in the rooftop HPHT scenario.

D. Link-to-System Mapping and Spectral Efficiencies

1) Methodology: Thus far, we have kept the link-level results distinct from the system-level results. However, to derive the achievable spectral efficiencies with the new numerology, a link-to-system mapping is in order. The way we do this is as follows:

- We perform link-level simulations with TDL-E channels (as agreed towards simulation assumptions in [2]) with an RMS delay spread of 45μs for HPHT1 and 35μs for MPMT, and with a Doppler spread of 1 Hz in both cases. These RMS delay spreads are obtained from the channels observed in the system-level simulations. Note that the maximum delay spread for these TDL-E channels is much larger than the RMS delay spreads—well beyond the cyclic prefix duration, and in cases, resulting in the last channel tap lying outside the equalization interval.
- Next, for each instance of the link-level simulation, we save the following quantities synchronously
  - Transport Block Error Map, i.e., whether that instance was a success or a failure
  - Instantaneous SNR Map, which is obtained following the same mapping as in the system-level simulations (see Section IV-B2 for SNR calculation)
- After collecting the above two arrays for all instances, we apply a binning on the instantaneous SNRs to generate the system-mapped BLER-vs-SNR curves that we present next.

2) System-Mapped Link-Level Results: The link-to-system mapped results for the MPMT and HPHT scenarios are depicted in Fig. 12.

Reading off the Transport Block Size (TBS) immediately to the left of the SNRs obtained from the corresponding system-level simulations (presented in Section IV-B), we can obtain the spectral efficiency for a given setting by dividing the TBS by the product of the system bandwidth (10 MHz in our evaluations) and symbol duration (3 milliseconds for the 300-microsecond CP numerology). The spectral efficiencies thus obtained are depicted below in Table I for 95 and 99 percent coverage, where the SNRs for 95 and 99 percent coverage are the system-level SNRs corresponding to the 95$^{\text{th}}$ and 99$^{\text{th}}$ percentile of SNRs that randomly deployed UEs may experience (as described in Section IV-B3) We observe from Table I that for a 95% coverage requirement, both for MPMT and HPHT scenarios, a spectral efficiency of approximately 2 bits/sec/Hz or higher is achievable with the new numerology. The spectral efficiency shown here, however, does not take into account any additional overheads that may arise from application layer forward error correction (AL-FEC) schemes that may be employed for MBMS.

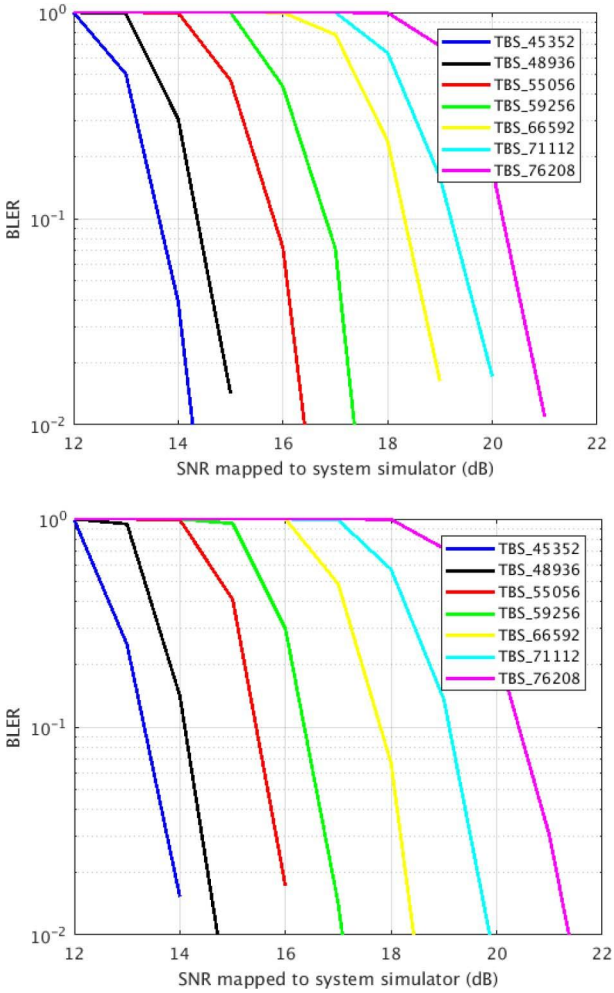

Fig. 12. System Mapped BLER performance: (a) MPMT rooftop scenario on the top and (b) HPHT rooftop scenario on the bottom.

V. Support for High Mobility up to 250 kmph

A. Numerology With 100 Microseconds Cyclic Prefix

As mentioned in Section III, one of the areas in which MBMS evolution took place in Release 16 was in the realm of providing support for high mobility of up to 250 kmph. It was decided to support a numerology with 100-microsecond cyclic prefix, which has twice the amount of Doppler resiliency as that of the Release 14 numerology with 200-microsecond

TABLE I
SPECTRAL EFFICIENCIES ACHIEVED

Scenario	System-level SNR (dB)	Best TBS decodable at 1% BLER (TBS_{max})	Spectral Efficiency (bps/Hz) $= \frac{TBS_{max}}{T_{symb} \times BW}$
MPMT (95% coverage)	19.9	66592	2.23
MPMT (99% coverage)	19.1	66592	2.23
HPHT (95% coverage)	18	59256	1.97
HPHT (99% coverage)	15.7	48936	1.63

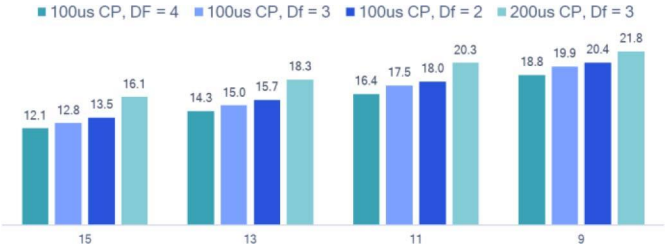

Fig. 13. System-level SNRs for car-mounted receivers in LPLT settings under the 50/1 ITU-R P.1546-5 channel model with small scale fading.

CP. This *high-mobility numerology* has a useful symbol duration of 400 microseconds, thereby resulting in two PMCH symbols per 1 millisecond subframe.

The target use case for this numerology is for car-mounted receivers in a LPLT setting—i.e., low-power low-tower transmitters with an ISD of up to 15 km.

B. System Level Evaluations

Fig. 13 presents the system-level SNRs obtained from using both the numerologies (200-microsecond CP and 100-microsecond CP) under different equalization internals and for different values of ISDs in a car-mounted LPLT setup. In the figure, each group of bars represents results for a given ISD (annotated by the ISD value in km below the corresponding group of bars).

From Fig. 13 we make the following observations: first, that a frequency spacing of $F_d = 2$ provides the best system-level performance for the 100-microsecond CP numerology. This is explained by the fact that the subcarrier spacing of this numerology is twice that of the 200-microsecond CP numerology, and as a result, to accurately estimate the channel, the RS density in frequency cannot be made sparser.

Second, we see that although the system-level SNRs obtained for the 200-microsecond CP numerology are always higher than that of the 100-microsecond CP numerology, the differences start to reduce as the ISDs become smaller. This is also to be expected, since the 100-microsecond CP inherently has less inter-symbol interference protection built in than the 200-microsecond CP—and the smaller the ISD, the lesser the delay spread of the channel, thereby closing the gap of the 100-microsecond CP numerology to the 200-microsecond CP numerology.

The system-level SNRs obtained here are only part of the overall story however. As we will show next, the loss in system-level SNR that the 100-microsecond CP numerology suffers, may be more than made up for when a combined link-and-system level analysis is performed. As alluded to before, the 100-microsecond CP numerology has a distinct advantage over its predecessor in terms of doppler-resiliency at high speeds—something that can only be demonstrated via link-level analysis.

C. Reference Signal Pattern

Owing to the high mobility use cases that this numerology caters to, it turns out to be suboptimal to use a large time-stagger pattern (as for the rooftop numerology described in the previous section) for the reference signals. This is because the channel changes very fast at such high speeds, and de-staggering and combing RSs from symbols further apart results in poor channel estimation performance. Furthermore, as seen above in the system level results, owing to the larger subcarrier spacing (2x that of the Release 14 numerology), a frequency spacing of $F_d = 2$ turned out to provide a better sampling of the underlying channel in the delay domain than a frequency spacing of $F_d = 3$. It was thus agreed to support a time and frequency stagger pattern of $F_d = 2, T_d = 2$ for this high-mobility numerology.

D. Comparison With Release 14 Numerology at 250 kmph

While the Release 14 numerology of 200-microsecond CP is good for most general-purpose scenarios of interest, its overall performance suffers at speeds of 250 kmph. This is illustrated in Fig. 14, where we see that even though the system-level SNRs achieved by the 100-microsecond CP numerology is 2.5 dB *lower* than that of the Release 14 numerology, this loss is more than compensated for by the link-level gains, on account of better doppler resiliency at higher speeds. A Transport Block of size 16416 bits does not converge to acceptable BLERs with the Release 14 numerology, while with the new 100-microsecond CP numerology, convergence to BLER = 10^{-2} occurs at $\approx$ 18 dB—in line with the system-level SNRs obtained for a car-mounted LPLT scenario with an ISD of 11km.

VI. ENHANCEMENTS TO THE CELL ACQUISITION SUBFRAME

A. Overview of CAS

As briefly described before in Section II-A, the Cell Acquisition Subframe (CAS) plays a key role in an LTE-based MBSFN transmission. In a dedicated MBMS carrier, the CAS occurs once every 40 milliseconds, and has the legacy LTE

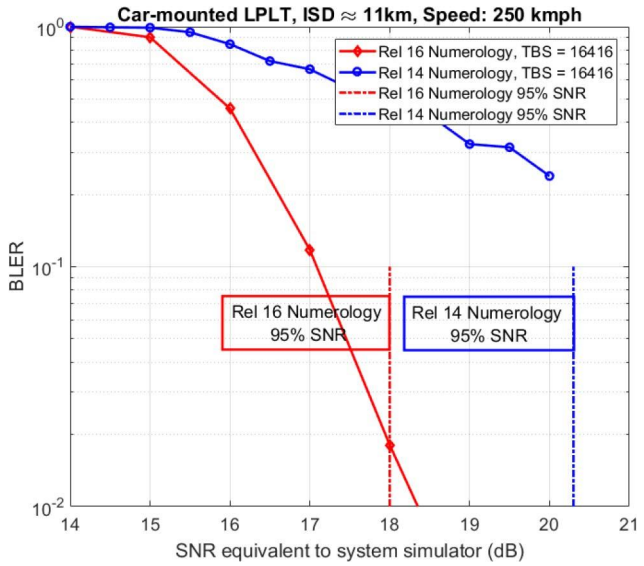

Fig. 14. Out performance of 100-microsecond CP numerology at 250 kmph.

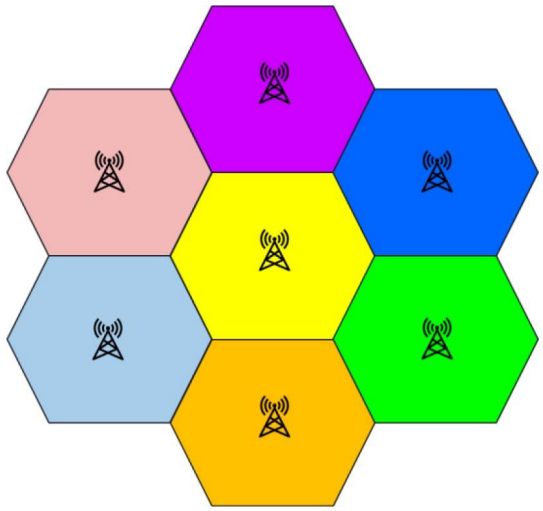

Fig. 15. Non-SFN CAS where the CASs from different transmitters (marked with different colors) are not synchronized.

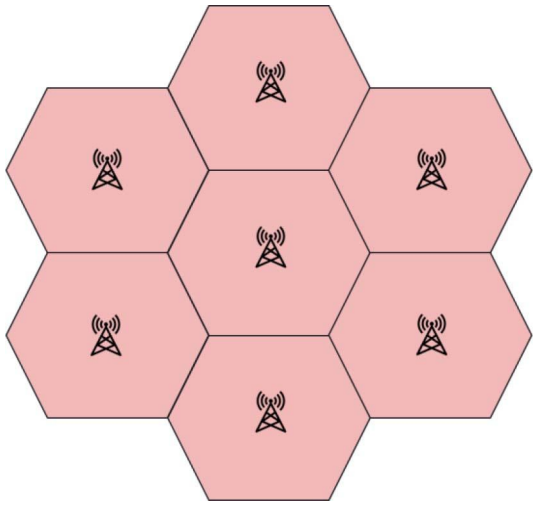

Fig. 16. SFN CAS with synchronized cells.

numerology of 15 kHz subcarrier spacing. The duration of the CAS is also 1 legacy LTE subframe—i.e., 1 millisecond. The CAS carries the synchronization signals, as well as the basic control and system information that a UE needs to receive the broadcast information from the MBSFN subframes.

In particular, the CAS carries the primary synchronization signal (PSS) and the secondary synchronization signal (SSS) which a UE uses to synchronize to a given cell, the physical broadcast channel (PBCH) which carries the Master Information Block (MIB), the Physical Downlink Control Channel (PDCCH) which carries (some) downlink control information, the Physical Control Format Indicator Channel (PCFICH), which conveys the number of OFDM symbols used for PDCCH and the Physical Downlink Shared Channel (PDSCH) which carries the System Information Blocks (SIBs) which the UE uses to determine the configuration of the Multicast Control Channels (MCCHs) associated with the MBSFN transmissions. For proper functioning of an LTE-based MBMS system, it is critical that a UE can decode all these channels in the CAS reliably.

B. SFN Versus Non-SFN CAS

CAS deployments may primarily be of two types: non-SFN CAS and SFN CAS. In non-SFN CAS deployments (example shown in Fig. 15), transmitters are not assumed to be tightly synchronized among each other for the purpose of CAS reception at a UE receiving MBMS. For non-sectorized (omni) transmitters, each transmitter has its own timing and interferes with all other transmitters, while for sectorized transmitters, the sectors of the same transmitter may be synchronized and form a mini-SFN. In non-SFN CAS deployments, CAS transmissions from other cells may cause interference to the CAS transmission in the cell in which a UE is receiving CAS. In contrast, in SFN CAS deployments (example shown in Fig. 16), all the transmitters are synchronized. This minimizes interference and improves the SNRs for the channels associated with the CAS.

SFN CAS, however, is challenging to deploy owing to the much tighter inter-transmitter synchronization requirements that arise from a 16.67 microsecond CP of the legacy 15 KHz numerology that is used for the CAS. This is in contrast to several numerologies for PMCH, where the CPs can be hundreds of microseconds long, leading to more relaxed inter-transmission synchronization requirements for SFN-based PMCH transmission. To this end, the system design should cater to the case of non-SFN CAS, wherein the CAS from other transmitters causes interference to the intended CAS. Typically, this is the limiting case for CAS design—a design that can ensure adequate coverage for non-SFN CAS will naturally satisfy the requirements for the SFN-CAS.

We would also like to note that an SFN-based transmission for the PMCH does not necessarily imply an SFN-CAS deployment. For the reasons described above, a typical deployment may often consist of a non-SFN CAS with SFN PMCH transmission.

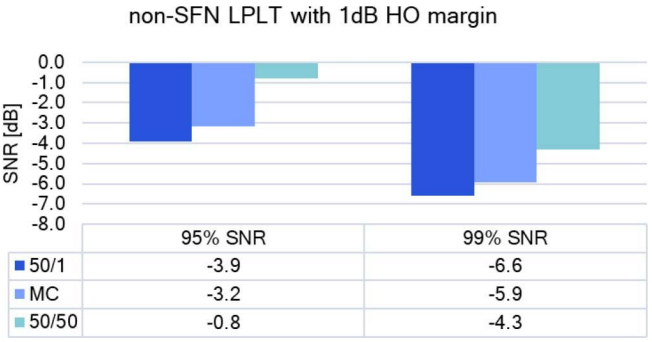

	95% SNR	99% SNR
50/1	-3.9	-6.6
MC	-3.2	-5.9
50/50	-0.8	-4.3

Fig. 17. System-level SNRs for non-SFN CAS for car-mounted LPLT receivers with small scale fading and 2 Rx antennas.

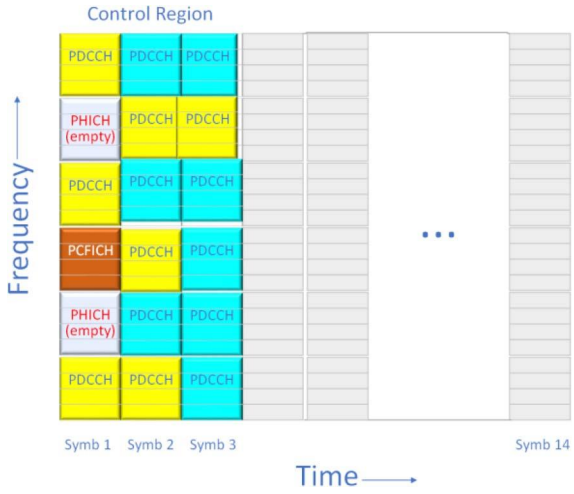

Fig. 18. Example CAS structure with a new AL16 PDCCH candidate. The cyan REs (or REGs) correspond to the bits generated beyond the legacy AL8 stream, from the rate matching algorithm. The contents of the yellow REGs are the same as legacy AL8.

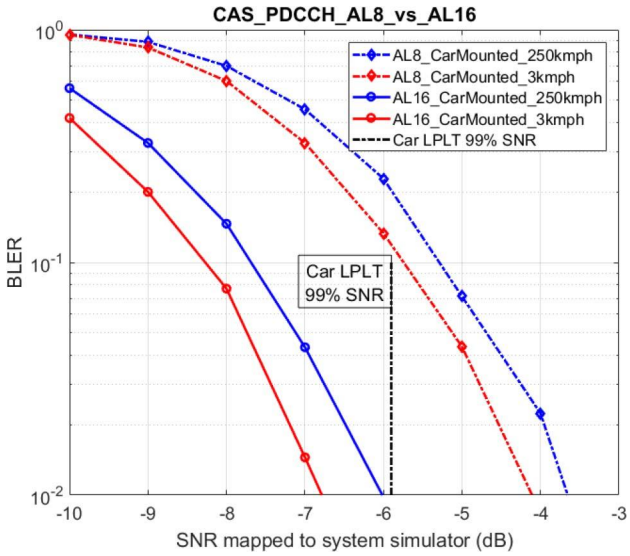

Fig. 19. Performance of Aggregation Level 8 and 16 for CAS-PDCCH in car-mounted LPLT scenarios.

C. System Level Evaluations

1) Channel Modeling for CAS: For receiving a non-SFN CAS, the P.1546-5 50/1 (serving/interfering) time-variability model (as described in Section IV-B1) turns out to be too pessimistic. This is in part because a mobile UE operating on 3GPP standards is capable of reselecting to a stronger cell, via a handover mechanism. Additionally, the model assumes that all the interferers are fully correlated, which is also unrealistic. To address these issues, a Monte Carlo (MC) simulation-based channel model was used for the non-SFN CAS evaluations that considers cell-reselection (with a 1 dB handover margin) and a random correlation coefficient between the transmitters. This MC channel model provides a more realistic view of the SNRs that a UE is likely to experience when receiving a non-SFN CAS.

2) Performance Evaluation: We see in Fig. 17 that the 99$^{\text{th}}$ percentile SNR (with the MC channel model) for the car mounted LPLT receiver (with 2 Rx antennas) is -5.9 dB. As we will see in the link-level evaluations that follow for the CAS, PDCCH decoding (and to some extent, PBCH decoding) is not possible with a 1% BLER at these SNR levels. This motivates the need to enhance the PDCCH and PBCH of the CAS.

D. Enhancements to PDCCH

1) PDCCH Candidate With Aggregation Level 16: In Legacy LTE (up to Release 15), the largest *aggregation level* (AL) of a PDCCH candidate was 8. Loosely speaking, an *aggregation level* of a PDCCH candidate determines a size of resource elements in the time-frequency grid over which the downlink control channel is mapped (for details, please see [4], [5]). To support PDCCH decoding with 1% BLER at -5.9 dB SNR, support for a PDCCH candidate with AL16 has been introduced in Release 16. This essentially doubles the maximum number of resource elements in the time-frequency grid to which a control channel can be mapped, thereby reducing the code-rate of the downlink control channel payload and facilitating decoding at lower SNRs.

To maintain backwards compatibility with legacy UEs (that are not aware of the new AL16 PDCCH candidate), the first 8 control channel elements (CCEs) of the AL16 PDCCH candidate are kept the same as that of a legacy AL8 candidate. An example depiction of such a PDCCH candidate is shown in Fig. 18.

2) Link Level Evaluations: Fig. 19 shows the performance of the CAS-PDCCH using legacy AL8 candidates and the newly introduced AL16 candidate. The -5.9-dB limiting threshold for the car-mounted LPLT receiver (described in Section VI-C) is also indicated in the figure. The AL16 candidate provides an almost 3 dB gain over the legacy AL8 candidate and more importantly, facilitates CAS-PDCCH decoding with 1% BLER for all speeds in the range of 3 kmph to 250 kmph.

E. Enhancements to PBCH

1) PBCH Repetitions: Like the CAS-PDCCH described above, it is important to ensure that the PBCH (which carries the MIB) can be decoded with 1% BLER at low SNRs typical

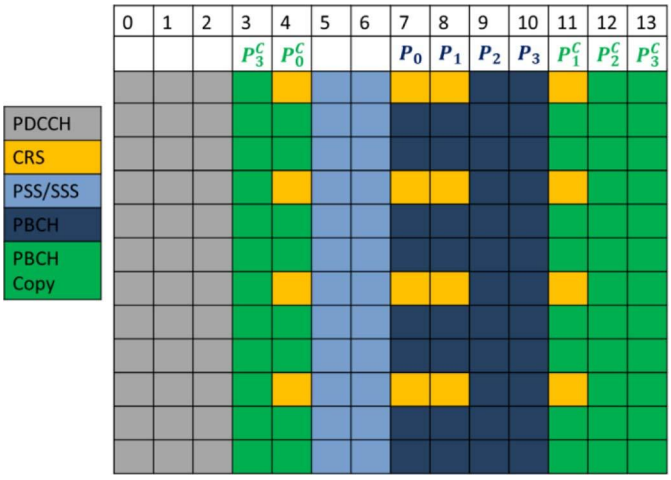

Fig. 20. PBCH symbol repetitions in a PRB within the center 6 PRBs of the CAS. Symbols P_i denote the original PBCH symbols, while the symbols P_i^C denotes the "copy" of PBCH symbol P_i. The symbol indices in the CAS subframe are indexed from 0–13.

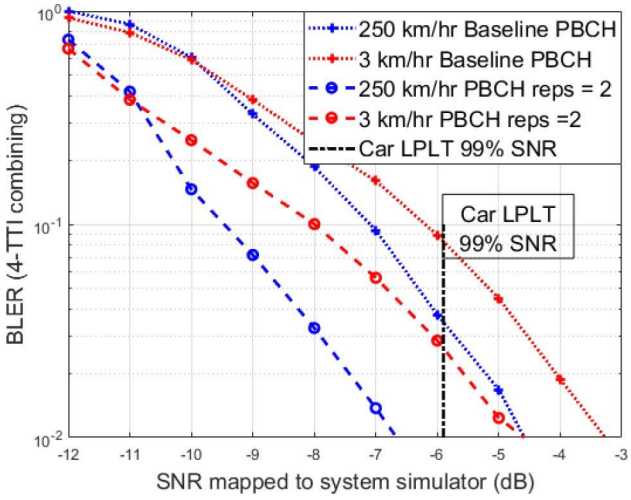

Fig. 21. Performance of CAS-PBCH with PBCH repetitions and 4-TTI combining in LPLT scenarios with car-mounted receivers.

of the car-mounted LPLT non-SFN CAS scenario. To this end, support for PBCH repetitions within the CAS was added for all but the lowest system bandwidth of 1.4 MHz. For system bandwidths greater than or equal to 5 MHz, PBCH repetitions are supported in all CAS subframes, while for the 3 MHz system, PBCH repetitions are supported in every alternate CAS subframe [9].

The PBCH symbol repetition pattern within a subframe follows the same structure as for bandlimited machine-type communication (MTC) UEs, as described in 3GPP TS 36.211 [4, Tab. 6.6.4-1]. The repetition pattern in a resource block within the center 6 physical resource blocks (PRBs) is depicted in Fig. 20.

2) Interference Randomization: For CAS reception, one is essentially operating in an *interference limited* regime—i.e., one where the interfering signal is much stronger than the noise. Thus, it is important that the interference from different cells appears as random as possible. This is facilitated in several applications (for example in the channels corresponding to NB-IoT in 3GPP TS 36.211 [4]) by means of *interference randomization*.

Applying the interference randomization paradigm to the PBCH repetitions described above, the copied symbols (marked in green in Fig. 20) are multiplied with a pseudo-random phase $\theta_{l,k}$ at symbol $l \in \{0, 1, \ldots, 13\}$ and subcarrier index $k \in \{0, 1, \ldots, 71\}$ (corresponding to the center 6 PRBs), where $\theta_{l,k}$ is given below:

$$\theta_{l,k} = \begin{cases} 1, & c_l(2k) = 0,\ c_l(2k+1) = 0 \\ -1, & c_l(2k) = 0,\ c_l(2k+1) = 1 \\ j, & c_l(2k) = 1,\ c_l(2k+1) = 0 \\ -j, & c_l(2k) = 1,\ c_l(2k+1) = 1 \end{cases}$$

In the above equation, it is assumed that $c_l(.)$ comes from a length-144 Gold sequence (per Clause 7.2, TS 36.211 [4]) that is initialized at symbol l with $c_{init,l} = 2^{13}((N_{ID} + 1) \times (1 + l + N_{DL}^{symb} n_s)) + 2^4 N_{ID} + (l + N_{DL}^{symb} n_s)$, where N_{DL}^{symb} denotes the number of symbols in a slot, and n_s denotes the slot index $\in \{0, 1\}$ in a given CAS subframe.

3) Link Level Evaluations: In Fig. 21, we depict the performance of the CAS-PBCH for different UE speeds, both with and without PBCH repetitions. We note that we achieve this BLER performance by using *4-TTI combining*, i.e., we make use of the fact the content of the MIB in the CAS doesn't change for 160 milliseconds (4 consecutive CAS occasions) and combine the LLRs corresponding to PBCH across the 4 CASs for decoding.

We observe in Fig. 21 that without PBCH repetitions, the BLER achieved for a (slow) UE moving at 3 kmph is around 9 percent, while that of a fast-moving UE is around 4 percent. With PBCH repetitions enabled, a fast-moving UE can achieve a BLER $< 1\%$, while even for a slow-moving UE (which sees limited time-diversity across the 4 consecutive CASs), the BLER reduces to around 3 percent.

F. Control Format Indication in MIB

The Physical Control Format Indicator Channel (PCFICH) indicates the number of OFDM symbols within the CAS that are designated for control channel (PDCCH) transmission. As such, reliable decoding of CFI information is essential for reliable PDCCH decoding. To this end, it was decided in Release 16 to support adding the control format indication (CFI) to the MIB by using two of the spare bits. This helps to enhance CAS reception since the support of MIB repetitions also increases the reliability of CFI.

VII. Conclusion

In this paper, we have provided an overview of the state-of-the art in 3GPP-based cellular terrestrial broadcasting techniques at the physical layer. We began with a brief overview of 3GPP Releases 9 through 14—eMBMS and FeMBMS—and subsequently proceeded to provide a detailed exposition on the most recent advances to cellular terrestrial broadcast in 3GPP Release 16. Among these, we have described how new numerologies with very long CPs have been introduced to facilitate rooftop reception with large area SFNs having ISDs of up to 125 km with significant improvement in system

level SNRs vis-à-vis using prior numerologies. Further, we described how 3GPP Release 16 added support for high mobility UEs with speeds of up to 250 kmph using car-mounted antennas. Next, we described multiple enhancements made to the physical layer control signal structure—namely, support for higher aggregation levels to improve PDCCH reliability, support of PBCH symbol repetitions and support for CFI in MIB—within the CAS for dedicated MBMS carriers. Together, these enhancements constitute a set of specifications that satisfy the requirements of 5G cellular broadcast as laid out in [1]. This, along with potential future work in forthcoming Releases of 3GPP, may serve to enable increasingly ubiquitous adoptions of 3GPP-based terrestrial broadcasting solutions by broadcasters around the world.

ACKNOWLEDGMENT

The authors would like to acknowledge the contributions of numerous colleagues and mentors at Qualcomm, including Thomas Stockhammer, Haris Zisimopoulos, Peter Gaal, Brian Banister, Aamod Khandekar, Qiang Shen, Arash Mirbagheri, Chu-Hsiang Huang, Le Liu, Umesh Phuyal and many others, whose technical insights and suggestions greatly improved the quality of work.

REFERENCES

[1] "Study on scenarios and requirements for next generation access technologies" 3GPP, Sophia Antipolis, France, Rep. 3GPP TR 38.913.
[2] "Study on LTE-based 5G terrestrial broadcast (release 16)" 3GPP, Sophia Antipolis, France, Rep. 3GPP TR 36.776.
[3] "Study on channel model for frequencies from 0.5 to 100 GHz" 3GPP, Sophia Antipolis, France, Rep. 3GPP TR 38.901.
[4] "Evolved Universal Terrestrial Radio Access (E-UTRA); Physical channels and modulation" 3GPP, Sophia Antipolis, France, Rep. 3GPP TS 36.211.
[5] "Evolved Universal Terrestrial Radio Access (E-UTRA); Physical layer procedures" 3GPP, Sophia Antipolis, France, Rep. 3GPP TS 36.213.
[6] "Method for Point-to-Area Predictions for Terrestrial Services in the Frequency Range 30 MHz to 3000 MHz," Int. Telecommun. Union, Geneva, Switzerland, ITU-Recommendation P.1546-5.
[7] "Frequency and Network Planning Aspects of DVB-T2" Int. Telecommun. Union, Geneva, Switzerland, ITU-Recommendation BT.2254-3.
[8] *On RS Pattern(s), MCS and UE Capabilities for the Numerology to Support Rooftop*, document 3GPP RANMeeting#199, R1-1911913, Huawei/HiSilicon, Shenzhen, China, 2019.
[9] *Potential Enhancement for CAS*, document 3GPP RANMeeting#199, R1-1911914, Huawei/HiSilicon, Shenzhen, China, 2019.
[10] *Digital Video Broadcasting (DVB); Frame Structure Channel Coding and Modulation for a Second-Generation Digital Terrestrial Broadcasting System (DVB-T2)*, ETSI Standard ETSI EN 302 755.
[11] *ATSC Standard: ATSC 3.0 System*. Standard A/300:2017, Oct. 2017.
[12] *Support of Longer Numerologies for Rooftop Reception*, document 3GPP RANMeeting#199, R1-1913247, Qualcomm Inc., San Diego, CA, USA, 2019.
[13] *Analysis of CAS Reception*, document 3GPP RANMeeting#199, R1-1912691, Qualcomm Inc., San Diego, CA, USA, 2019.
[14] *Analysis of CAS Reception*, document 3GPP RANMeeting#196bis, R1-1904535, Qualcomm Inc., San Diego, CA, USA, 2019.
[15] D. Lecompte and F. Gabin, "Evolved multimedia broadcast/multicast service (eMBMS) in LTE-advanced: Overview and rel-11 enhancements," *IEEE Commun. Mag.*, vol. 50, no. 11, pp. 68–74, Nov. 2012.
[16] A. Urie, A. N. Rudrapatna, C. Raman, and J.-M. Hanriot, "Evolved multimedia broadcast multicast service in LTE: An assessment of system performance under realistic radio network engineering conditions," *Bell Lab. Tech. J.*, vol. 18, no. 2, pp. 57–76, Sep. 2013.
[17] A. Awada, M. Säily, and L. Kuru, "Design and performance impact of long cyclic prefixes for eMBMS in LTE networks," in *Proc. IEEE Wireless Commun. Netw. Conf.*, Doha, Qatar, 2016, pp. 1–7.
[18] L. Zhang, Y. Wu, G. K. Walker, W. Li, K. Salehian, and A. Florea, "Improving LTE *e*MBMS with extended OFDM parameters and layered-division-multiplexing," *IEEE Trans. Broadcast.*, vol. 63, no. 1, pp. 32–47, Mar. 2017.
[19] J. J. Gimenez, P. Renka, S. Elliott, D. Vargas, and D. Gomez-Barquero, "Enhanced TV delivery with EMBMS: Coverage evaluation for rooftop reception," in *Proc. IEEE Int. Symp. Broadband Multimedia Syst. Broadcast. (BMSB)*, Valencia, Spain, 2018, pp. 1–5.
[20] L. Richter and S. Ilsen, "Coverage evaluation of LTE FeMBMS: A case study based on a DVB-T2 network," in *Proc. IEEE Int. Symp. Broadband Multimedia Syst. Broadcast. (BMSB)*, Valencia, Spain, 2018, pp. 1–5.
[21] Y. Xu *et al.*, "Enhancements on coding and modulation schemes for LTE-based 5G terrestrial broadcast system," *IEEE Trans. Broadcast.*, early access, Apr. 3, 2020, doi: 10.1109/TBC.2020.2981772.
[22] D. He *et al.*, "Study on new numerology and CAS enhancement for LTE-based 5G terrestrial broadcast," *IEEE Trans. Broadcast.*, 2020.
[23] D. Gomez-Barquero, D. Navratil, S. Appleby, and M. Stagg, "Point-to-multipoint communication enablers for the fifth generation of wireless systems," *IEEE Commun. Standards Mag.*, vol. 2, no. 1, pp. 53–59, Mar. 2018.
[24] J. J. Gimenez, D. Gomez-Barquero, J. Morgade, and E. Stare, "Wideband broadcasting: A power-efficient approach to 5G broadcasting," *IEEE Commun. Mag.*, vol. 56, no. 3, pp. 119–125, Mar. 2018.
[25] J. J. Gimenez *et al.*, "5G new radio for terrestrial broadcast: A forward-looking approach for NR-MBMS," *IEEE Trans. Broadcast.*, vol. 65, no. 2, pp. 356–368, Jun. 2019.
[26] I. Eizmendi *et al.*, "DVB-T2: The second generation of terrestrial digital video broadcasting system," *IEEE Trans. Broadcast.*, vol. 60, no. 2, pp. 258–271, Jun. 2014.
[27] L. Fay, L. Michael, D. Gómez-Barquero, N. Ammar, and M. W. Caldwell, "An overview of the ATSC 3.0 physical layer specification," *IEEE Trans. Broadcast.*, vol. 62, no. 1, pp. 159–171, Mar. 2016.